Structure of the single-strand annealing domain of human RAD52 protein

Martin R. Singleton, Lois M. Wentzell*, Yilun Liu, Stephen C. West, and Dale B. Wigley†

Cancer Research U.K., London Research Institute, Clare Hall Laboratories, South Mimms, Hertfordshire EN6 3LD, United Kingdom

Edited by Nicholas R. Cozzarelli, University of California, Berkeley, CA, and approved August 28, 2002 (received for review July 29, 2002)

In eukaryotic cells, RAD52 protein plays a central role in genetic recombination and DNA repair by (*i*) promoting the annealing of complementary single-stranded DNA and (*ii*) stimulation of the RAD51 recombinase. The single-strand annealing domain resides in the N-terminal region of the protein and is highly conserved, whereas the nonconserved RAD51-interaction domain is located in the C-terminal region. An N-terminal fragment of human RAD52 (residues 1–209) has been purified to homogeneity and, similar to the full-size protein (residues 1–418), shown to promote single-strand annealing *in vitro*. We have determined the crystal structure of this single-strand annealing domain at 2.7 Å. The structure reveals an undecameric (11) subunit ring with extensive subunit contacts. A large, positively charged groove runs along the surface of the ring, readily suggesting a mechanism by which RAD52 presents the single strand for reannealing with complementary single-stranded DNA.

recombination | DNA repair | crystallography

The ability of a cell to survive agents that promote genome breakage requires efficient recombinational repair systems. In lower eukaryotes, repair involves the *RAD52* epistasis group of genes including *RAD50*, *RAD51*, *RAD52*, *RAD54*, *RAD55*, *RAD57*, *RAD59*, *MRE11*, and *XRS2* (1, 2). A key member of this group, *RAD52*, encodes a protein that plays a dual role in recombination by (*i*) promoting the annealing of complementary single strands (3–5) and (*ii*) stimulating *in vitro* recombination reactions catalyzed by the RAD51 recombinase (6–8).

Human RAD52 protein shares many properties with its yeast counterpart including DNA strand annealing and RAD51 stimulation activities (9–11). The human protein has been visualized by electron microscopy, and a low-resolution three-dimensional structure has been determined (12, 13). Human RAD52 consists of seven subunits that are organized in the form of a ring with a large central channel. The *Saccharomyces cerevisiae* RAD52 protein has been shown also to form rings, but no detailed structure is available presently (4).

The mechanism by which RAD52 promotes single-stranded DNA (ssDNA) annealing is unknown. However, when complexes formed between RAD52 and ssDNA were probed with hydroxyl radicals, a unique repeating four-nucleotide hypersensitivity pattern was observed (14). Sequence-independent hypersensitivity was observed over ≈36 nucleotides and was phased precisely from the terminal nucleotide. These results led to the proposal that RAD52 binds ssDNA via specific interactions with the terminal base, leading to the formation of a precisely organized ssDNA–RAD52 complex in which the DNA lies on an exposed surface of the protein ring.

Sequence comparisons, site-directed mutagenesis, and biochemical studies indicate that the highly conserved N-terminal region of RAD52 possesses ssDNA annealing activities, whereas the RAD51-interaction domain is located toward the nonconserved C-terminal region (15–18). Furthermore, the RAD59 protein shares sequence homology with the N-terminal region of RAD52 but lacks the C-terminal domain. RAD59 catalyzes strand annealing *in vitro* (19). To gain insight into the mechanism of single-strand annealing promoted by RAD52, we have purified an N-terminal fragment of human RAD52 (residues 1–209) and show that the truncated protein promotes single-strand annealing but is unable to stimulate the recombination activities of RAD51. The structure of $RAD52_{1–209}$ has been solved at a resolution of 2.7 Å, revealing an 11-subunit ring. A groove that runs across the surface of the undecamer and is lined by conserved basic residues is likely to be the DNA-binding site. A mechanism for ssDNA-strand annealing is discussed.

Experimental Procedures

Proteins for Biochemical Studies. Full-length human RAD52 was purified from baculovirus-infected Sf9 cells as described (12). To produce His-tagged $RAD52_{1–209}$, the N-terminal region of the human *RAD52* gene was PCR-amplified and cloned into the *Nde*I and *Bam*HI sites of pET15b (Novagen). The recombinant protein was purified from 4 liters of FB850 pLysS carrying pET15b-$RAD52_{1–209}$ grown in LB medium containing 100 μg/ml carbenicillin and 25 μg/ml chloramphenicol. At OD_{600} = 0.5, RAD52 synthesis was induced by using 1 mM isopropyl-β-D-thiogalactoside, and 4 h later the cells were harvested by centrifugation. The cell pellet was resuspended in 200 ml of T buffer (20 mM Tris·HCl, pH 8.0/0.5 M NaCl/10% glycerol/0.02% Triton X-100) containing 5 mM imidazole (T5), 0.2 mg/ml phenylmethylsulfonyl fluoride, and aprotinin (0.016 trypsin units/ml). The suspension was divided into 4 × 50 ml aliquots and sonicated (three times for 30 sec). The cell debris was removed by centrifugation in a Beckmann 45 Ti rotor at 35,000 rpm for 1 h at 4°C.

The supernatant was loaded onto a 20-ml Talon column (CLONTECH) preequilibrated with T5 buffer. The column was washed with 200 ml of T buffer containing 40 mM imidazole, and the protein was eluted with a 200-ml gradient of 40–500 mM imidazole in T buffer. Fractions containing $RAD52_{1–209}$ were identified by SDS/PAGE, and peak fractions were pooled. The pool then was diluted to reduce the NaCl concentration to 200 mM and loaded onto a 25-ml Heparin column (Bio-Rad, Affigel) preequilibrated with R buffer (20 mM Tris·HCl, pH 8.0/10% glycerol/0.5 mM DTT) containing 200 mM KCl (R200). The column was washed with R200 buffer, and proteins were eluted with a linear KCl gradient. $RAD52_{1–209}$ was pooled, diluted in R buffer to reduce the KCl concentration to 0.2 M, and loaded onto an ssDNA cellulose column (Sigma–Aldrich) preequilibrated with R200 buffer. The column was washed with four successive washes of 40 ml of R200 buffer, 32 ml of R200 containing 1 mM ATP, 28 ml of R200 containing 0.5 mM $MgCl_2$ and 2 mM ATP (to remove a heat-shock protein contaminant), and finally 40 ml of R200 buffer. The protein was eluted by using a 39-ml gradient of 0.2–1.0 M KCl in R buffer. Peak fractions were pooled and

This paper was submitted directly (Track II) to the PNAS office.

Abbreviations: ssDNA, single-stranded DNA; RPA, replication protein A.

Data deposition: The atomic coordinates and structure factors have been deposited in the Protein Data Bank, www.rcsb.org (PDB ID code 1H2I).

*Present address: GSK Clinical Pharmacology Unit, 51 North 39th Street, Philadelphia, PA 19104.

†To whom correspondence should be addressed. E-mail: dale.wigley@cancer.org.uk.

dialyzed for 90 min against 2 liters of 20 mM Tris·HCl, pH 8.0/10% glycerol/200 mM KCl/0.5 mM DTT/0.5 mM EDTA in 2-ml Slide-A-Lyzer dialysis cassettes (Pierce). The protein was divided into aliquots and stored at −80°C. Protein concentration was determined by using the Bradford assay with BSA as a standard. The final yield of protein was ≈12 mg.

Oligonucleotides. The oligonucleotides poly(dT)$_{40}$, SW436, and SW437 were purified by denaturing PAGE. The oligos used were 5′-TATCGAATCCGTCTAGTCAACGCTGCCGACATCTACGATTGACGTTTGGGCTCCTCGCAAGTCATTGG-3′ (SW436) and 5′-CCAATGACTTGCGAGGAGCCCAAACGTCAATCGTAGATGTCGGCAGCGTTGACTAGACGGATTCGATA-3′ (SW437).

All oligonucleotide concentrations are expressed in moles of nucleotides. DNA was 5′-^{32}P end-labeled by using T4 polynucleotide kinase (NEB, Beverly, MA) and [γ-^{32}P]ATP. Proteins were removed by phenol-chloroform extraction, and the DNA was passed through a G25 spin column (Amersham Pharmacia) to remove unincorporated nucleotides.

Hydroxyl-Radical Footprinting. Reactions contained 5′-^{32}P-labeled poly(dT)$_{40}$ (40 nM), binding buffer (50 mM triethanolamine HCl, pH 7.5/0.5 mM Mg(OAc)$_2$/1 mM DTT/100 μg/ml BSA), and RAD52 or RAD52$_{1–209}$ in a total volume of 100 μl. Because glycerol inhibits hydroxyl-radical formation, proteins were diluted in buffer lacking glycerol. DNA–protein complexes were incubated at 37°C for 20 min, and hydroxyl radicals were generated by the addition of 10 μl of each of the following freshly prepared solutions: Fe(II)·EDTA [0.2 mM Fe(II)/0.4 mM EDTA], 20 mM sodium ascorbate, and 0.6% H_2O_2. After 10 min the reactions were stopped by the addition of 15 mM thiourea and 3 mM EDTA, and the products were extracted with phenol chloroform and ethanol-precipitated. DNA products were analyzed by 12% denaturing PAGE and detected by autoradiography.

Single-Strand Annealing Assays. Reactions contained 5′-^{32}P-labeled oligo SW437 (200 nM), binding buffer (as described above), unlabeled oligo SW436 (200 nM), and full-length or truncated RAD52 in a total volume of 10 μl. All components except SW436 were mixed and incubated at 30°C for 5 min. Reactions were initiated by the addition of SW436, and after 2 min the reaction was stopped by the addition of a 10-fold excess of unlabeled SW437. SDS loading buffer [1× TAE (40 mM Tris base/1.1% vol/vol acetic acid/1 mM EDTA) 50% glycerol/0.1% SDS, 4 μl] was added to each sample, and the reaction products were analyzed by 10% nondenaturing PAGE and visualized by autoradiography.

Homologous Pairing and Strand-Exchange Assays. Single-stranded circular ϕX174 DNA (30 μM nucleotides) was preincubated with RAD52 (2 μM) or RAD52$_{1–209}$ (2 μM) for 5 min at 37°C, and RAD51 (1 μM) and replication protein A (RPA) (1 μM) were subsequently added at 5-min intervals. The reaction was initiated by the addition of ϕX174 *Apa*LI-linearized double-stranded DNA (30 μM). The final reaction (10 μl) contained 40 mM Tris·HCl, pH 7.8, 2 mM ATP, 1 mM $MgCl_2$, 1 mM DTT, 100 mM $(NH_4)_2SO_4$, 8 mM creatine phosphate, and 28 μg/ml creatine kinase. Incubation was carried out at 37°C for 1.5 h and terminated by the addition of one-fifth volume of stop buffer (100 mM Tris·HCl, pH 7.5/100 mM $MgCl_2$/30 mg/ml SDS/10 mg/ml proteinase K). The DNA was deproteinized by incubation at 37°C for 20 min and analyzed on 0.8% agarose gel in TAE buffer. The DNA was detected by using SYBR green I and PhosphorImaging (20).

Protein for Structural Studies. For the crystal-structure determination, the gene encoding RAD52$_{1–209}$ was cloned into pET22a without a polyhistidine tag. Expression of the protein was carried out in *Escherichia coli* BL21 cells carrying a plasmid (pSJS1240, a gift from S. J. Sandler, University of Massachusetts, Amherst) to express low-abundance tRNAs (21). Expression was induced by the addition of 1 mM isopropyl-β-D-thiogalactoside, and the cells were harvested and lysed by sonication into buffer A (50 mM Tris·HCl pH 7.5/200 mM NaCl/1 mM EDTA/2 mM DTT). Protein was precipitated by the addition of $(NH_4)_2SO_4$ to 60% saturation, redissolved in buffer A + 0.9 M $(NH_4)_2SO_4$, and then applied to a HiPrep low-substitution phenyl-Sepharose column (AP Biotech), and the RAD52$_{1–209}$ was eluted by a 0.9–0 M $(NH_4)_2SO_4$ gradient. The peak fractions were pooled, precipitated in 60% saturation $(NH_4)_2SO_4$ and loaded onto a Superdex 200 16/60 gel filtration column (AP Biotech) preequilibrated in buffer A. The peak fractions of RAD52$_{1–209}$ were applied to a HiTrap heparin affinity column (AP Biotech, Amersham, U.K.) and eluted with a 0.2–1.0 M NaCl gradient in buffer A.

Crystallization. For crystallization purposes, RAD52$_{1–209}$ was concentrated to 10 mg/ml in 10 mM Tris·HCl, pH 7.5/300 mM NaCl/1 mM DTT. Crystallization was carried out by using the hanging-drop vapor-diffusion method against a reservoir of 100 mM Tris·HCl, pH 8.0/4–14% (vol/vol) ethanol. Crystals usually appeared within 3 days and grew to a size of 0.1 × 0.3 × 0.3 mm. For cryocooling, the crystals were sequentially transferred to a solution of 100 mM Tris·HCl, pH 8.0/35% (vol/vol) ethylene glycol in steps of 5%.

Crystal Structure Determination. Crystals were of the monoclinic space group $P2_1$ with unit cell dimensions of a = 117.3 Å, b = 127.3 Å, c = 191.2 Å, and β = 90.3°. There are two undecameric protein complexes in the asymmetric unit. Data were collected from flash-frozen crystals at 100 K on a rotating anode source (native and mercury data) or at European Synchrotron Radiation Facility beamline 14.4 (selenium data) and processed by using the HKL programs (ref. 22; Tables 1 and 2). The structure was solved by using data from a selenomethionine-derivatized protein crystal combined with data from a mercury derivative described in Table 1. The 22 selenium sites (one per subunit) were identified by using SHAKE-AND-BAKE (23), and phases calculated from this derivative were used to identify 19 sites in the mercury derivative. Unless otherwise stated, the CCP4 program suite was used for the structure determination and subsequent manipulations (24). Initial phases were very poor but were improved significantly by density averaging using matrices derived from the heavy atom positions, combined with solvent

Table 1. Crystallographic statistics: Data collection

	Native	Mercury	Selenium
Resolution, Å	30–2.7	30–3.3	30–3.2
Completeness, % overall (2.8–2.7 Å)	97.0 (96.7)	99.0	97.0
I/σ (2.8–2.7 Å)	14.0 (2.7)		
R_{symm}, % overall (2.8–2.7 Å)	5.5 (27.9)	8.0	10.0
R_{deriv}, % overall	—	19.8	14.9
No. of sites	—	19	22
Phasing power	—	0.5	0.3
Overall mean figure of merit:	0.25		

Table 2. Crystallographic statistics: Final model

R_{factor} (all data), %	22.5
R_{free} (5% of data), %	26.2
rms deviation bond length, Å	0.014
rms deviation bond angle, °	1.78

BIOCHEMISTRY

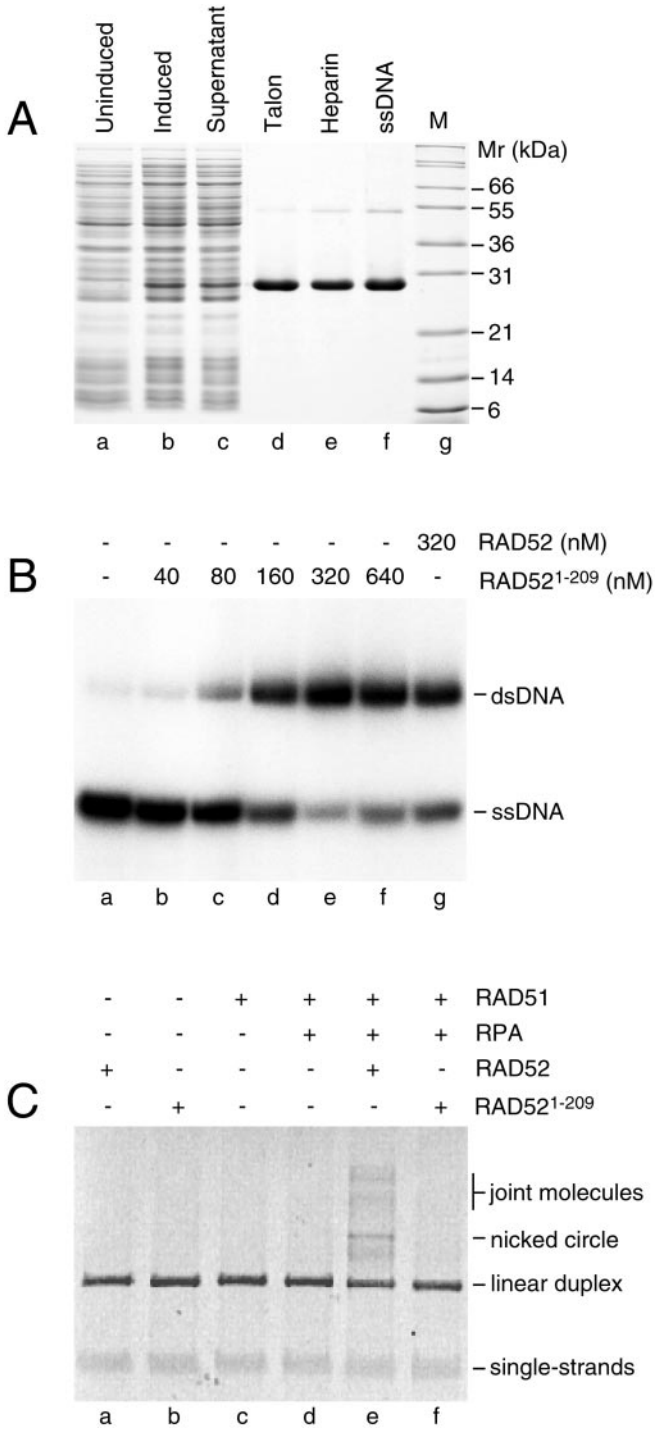

Fig. 1. Biochemical activities of $RAD52_{1–209}$. (*A*) Purification of His-tagged $RAD52_{1–209}$. Recombinant protein was overexpressed in *E. coli* and purified by chromatography on Talon, affi-gel heparin, and ssDNA cellulose as described in *Experimental Procedures*. Lane M, molecular mass markers. (*B*) Annealing of complementary ssDNAs by $RAD52_{1–209}$. Reactions contained two complementary oligonucleotides, of which one was ^{32}P-labeled. The products were analyzed by neutral PAGE as described in *Experimental Procedures*. dsDNA, double-stranded DNA. (*C*) $RAD52_{1–209}$ is defective in its ability to stimulate recombination reactions promoted by RAD51. Reactions containing single-stranded circular and linear duplex ϕX174 DNA were supplemented with the indicated proteins as described in *Experimental Procedures*, and the products of incubation were analyzed by agarose-gel electrophoresis. The DNA was visualized by staining with SYBR green and PhosphorImaging. The positions of joint molecules, linear duplex, and nicked circular-DNA products were determined by comparison with DNA markers (not shown).

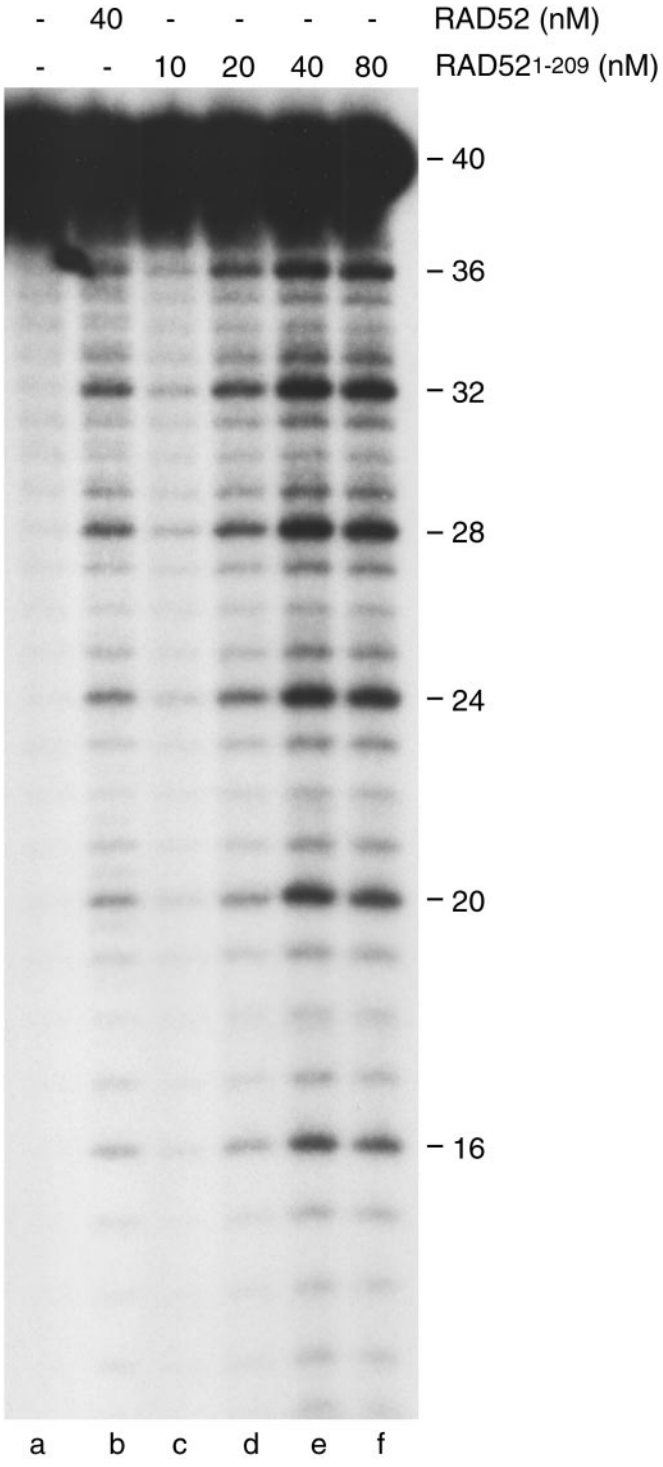

Fig. 2. Hypersensitivity of ssDNA bound by $RAD52_{1–209}$ to hydroxyl radicals. 5′-^{32}P-labeled poly(dT)$_{40}$ was incubated with the indicated concentrations of RAD52 or $RAD52_{1–209}$, and the products were probed with hydroxyl radicals as described in *Experimental Procedures*. ^{32}P-labeled products were analyzed by denaturing PAGE and autoradiography.

flattening in the program DM. Model building was undertaken by using TURBOFRODO (25). The positions of one methionine residue and one cysteine residue in each subunit were based on the observed heavy atom-binding sites. Model refinement was undertaken with CNS (26) interspersed with rounds of model building. Statistics concerning the quality of the final model are presented in Table 2.

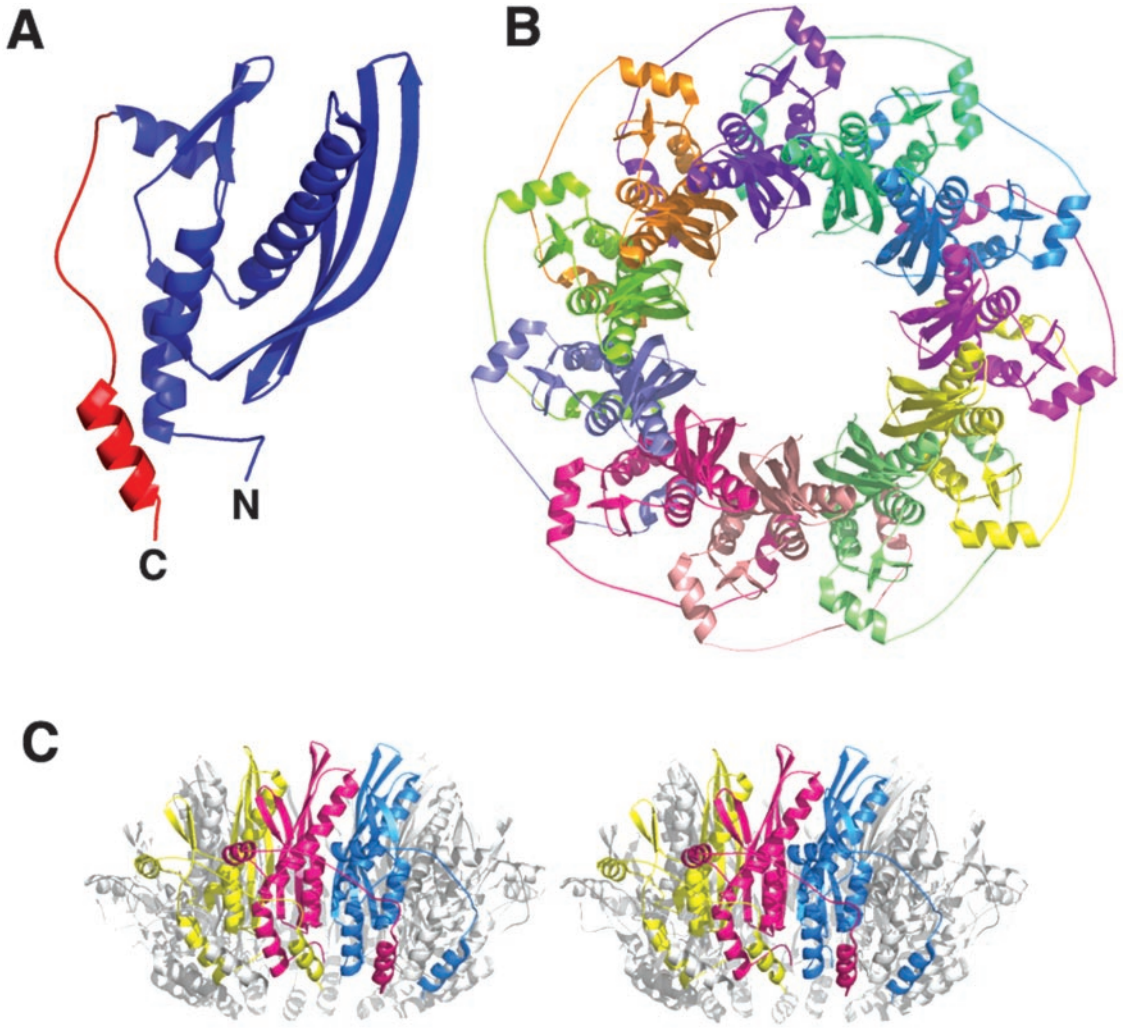

Fig. 3. Structure of the $RAD52_{1–209}$ undecamer. (*A*) Overall fold of the protein monomer. Domain 1 (residues 24–177) is colored blue, and domain 2 (residues 178–209) is colored red. (*B*) The undecamer viewed along the 11-fold symmetry axis. (*C*) Stereo image of the subunit contacts viewed at 90° from the view in *B*. Three adjacent subunits are shown in yellow, red, and blue to illustrate the subunit contacts. The remainder of the undecamer is shown in gray. This figure (and Figs. 4 and 5) was prepared by using PYMOL (http://pymol.sourceforge.net).

Results and Discussion

Biochemical Properties of $RAD52_{1–209}$. To isolate the domain of RAD52 that promotes single-strand annealing, the N-terminal region of human RAD52, comprising amino acids 1–209, was cloned into the expression vector pET15b. After overexpression in *E. coli*, $RAD52_{1–209}$ was purified to homogeneity (Fig. 1*A*). The 23-kDa protein, the identity of which was confirmed by amino acid sequencing, was found to migrate more slowly than predicted from its size. Analysis by SDS/PAGE also revealed the presence of dimeric $RAD52_{1–209}$, indicating that the truncated protein retained the expected ability to self-associate.

When $RAD52_{1–209}$ was incubated with two complementary single-stranded oligonucleotides, in which one was 5′-^{32}P end-labeled, we observed the formation of duplex DNA products (Fig. 1*B*). The N-terminal fragment of RAD52 was as efficient as the full-size RAD52 protein in promoting single-strand annealing *in vitro* (Fig. 1*B*, compare lane e with g, and data not shown). As observed previously for full-length RAD52 (11), excess $RAD_{1–209}$ was found to inhibit single-strand annealing. Whether this is because of the fact that the mechanism of annealing involves interactions between an ssDNA–RAD52 complex and naked ssDNA or is a consequence of nonspecific aggregation leading to nonproductive complex formation remains to be determined.

Because the RAD51-interaction domain is thought to be located in the C-terminal region of RAD52, which has been deleted from $RAD52_{1–209}$, we next determined whether the N terminus of RAD52 retained any ability to stimulate RAD51-mediated pairing reactions. Homologous pairing reactions between single-stranded circular and homologous linear duplex DNA were carried out at concentrations of RAD51 that were suboptimal for activity, because it has been shown that stimulation of RAD51 by RAD52 is most apparent under such conditions. As shown in Fig. 1*C*, the combined actions of RAD51 and RAD52 (in the presence of RPA) led to the formation of recombination intermediates and nicked circular-duplex products (lane e). These reactions showed an absolute requirement for RPA, because they were carried out in the presence of ammonium sulfate as described (27). The nicked circles result from a complete strand-exchange reaction in which the complementary strand of the linear duplex (5386 nucleotides in length) is transferred to the ssDNA circle. Under these suboptimal conditions, neither RAD51 nor RAD52 protein alone were able to catalyze homologous pairing (lanes a, c, and d). In contrast to the full-size RAD52 protein, over a range of biochemical

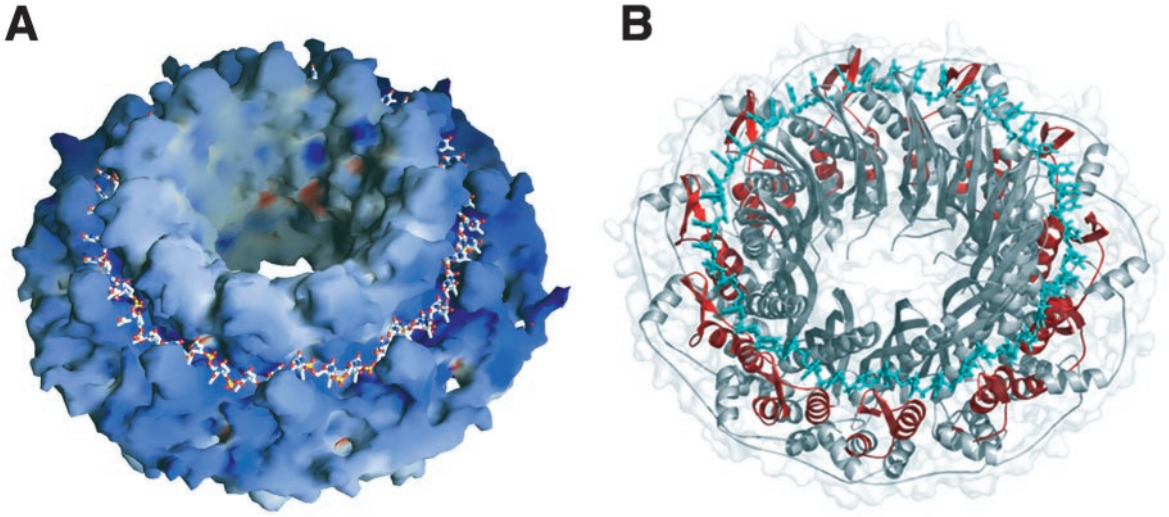

Fig. 4. Molecular surface of the protein. (*A*) Electrostatics of the molecular surface of the protein as determined in GRASP (30). Negative potential is shown in red, and positive potential is shown in blue. A deep groove that runs across the protein surface suggests a possible binding site for DNA. Modeled ssDNA is overlaid for reference. (*B*) A ribbon representation of the undecamer with modeled DNA (in cyan). Residues proposed to be involved in binding to DNA (residues 39–80) are shown in red with the remainder of the molecule shown in gray. The molecular boundary is shadowed in pale gray.

conditions, we found that $RAD52_{1–209}$ was unable to stimulate RAD51 to promote homologous pairing and strand exchange (lane f).

The binding of RAD52 to ssDNA results in the formation of a RAD52–ssDNA complex in which the DNA backbone is uniquely hypersensitive to attack by hydroxyl radicals (14). As shown in Fig. 2 (lane b) using $poly(dT)_{40}$, hypersensitivity was observed as a repeating four-nucleotide ladder along the entire length of the DNA. We proposed previously that this unique pattern is a consequence of the way in which ssDNA lies in an exposed groove on the surface of the RAD52 ring such that the phosphodiester backbone is distorted and exposed to solvent. Such an arrangement may be a critical feature that is required for single-strand annealing.

Because $RAD52_{1–209}$ retains the ability to self-associate and promote ssDNA annealing, we next determined whether this N-terminal fragment would impose the unique hydroxyl-radical sensitivity to bound ssDNA. We found that $RAD52_{1–209}$ induced the same hypersensitivity pattern as the full-length protein (Fig. 2, lanes c–f) and conclude that the ssDNA-binding groove in the full-length RAD52 ring remains intact in $RAD52_{1–209}$.

Overall Fold of $RAD52_{1–209}$. $RAD52_{1–209}$ comprises two structural domains (Fig. 3*A*). Domain 1 (residues 24–177, the N-terminal 23 residues of the protein are disordered) forms the core of the structure and has a mixed α/β structure. The smaller C-terminal domain 2 (residues 178–209) consists of a flexible, extended linker region that ends in an α-helix. Domain 2 extends from the surface to interact with domain 1 in an adjacent subunit.

The subunits are assembled as an undecamer in an 11-fold symmetric ring (Fig. 3*B*) with a large channel running through the center. The channel is wider at one end than the other with dimensions quite similar to those reported for the electron microscopy images of the full-length RAD52 heptamer (13).

Subunit Interface. The subunit contacts involve interactions between β-strands such that a continuous β-sheet extends around the entire molecule. Additional contacts are provided by the C-terminal helix (residues 197–209) that swaps across the domain boundary and interacts with an adjacent subunit in each case (Fig. 3*C*). The use of "helix swapping" to stabilize subunit interactions is a common feature in many oligomeric proteins including other ring proteins such as helicases (28). The shorter N-terminal fragment studied previously (29) only comprised residues 1–192 and as such will be missing the C-terminal helix that seems to form an important part of the subunit interface.

Different studies of the oligomeric assembly of RAD52 using scanning transmission electron microscopy (STEM) analysis on the full-length protein are in broad agreement. One study suggests a spread of oligomeric states between 4 and 13 subunits with an average of $\approx 6 \pm 1$ (29), whereas for the other the spread is a little less (4–10 subunits) with a mean of 7 ± 1 (13). By contrast, STEM analysis of an N-terminal fragment of RAD52 (residues 1–192) suggests oligomers of between 4 and 15 subunits with an average of 10 ± 1 subunits (29). Electron-microscopy studies of the full-length RAD52 molecule have produced a three-dimensional reconstruction with seven subunits in a ring (13).

The nature of the subunit interface probably can explain the

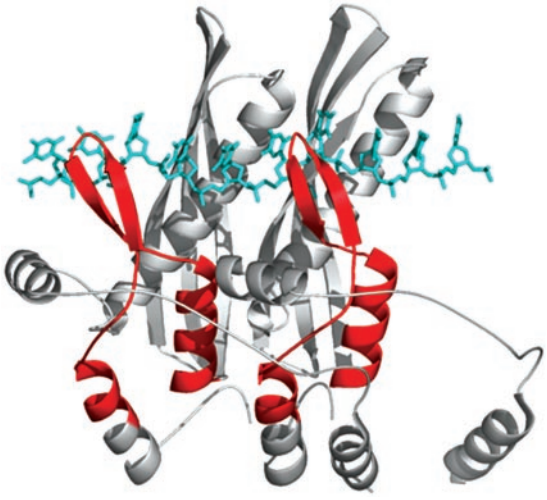

Fig. 5. ssDNA-binding site. Ribbon representation of the proposed ssDNA-binding site spanning two adjacent subunits. Residues 39–80 of the protein are colored red with the remainder shown in gray. The ssDNA is overlaid in cyan.

heterogeneous oligomeric nature of this fragment. The interface is formed in such a way that very similar contacts could be made if the protein were in a variety of oligomeric states. The subunit rotation required to form a sevenfold ring (51°) differs from that required for an 11-fold ring (33°) by only 18°. Presumably, in the full-length protein there are additional contacts made between the RAD51-binding domains that favor the sevenfold over the 11-fold ring, because the helix swapping observed suggests that the C-terminal region of the protein probably interacts with an adjacent subunit.

Potential DNA-Binding Site. Calculation of the molecular surface of the protein complex was carried out by using the GRASP program (30). This analysis revealed a deep groove on the protein surface that runs continuously around the outside of the ring (Fig. 4*A*). The residues lining this groove are highly conserved in RAD52 proteins from a variety of species. Residues at the base of the cleft are positively charged, whereas those lining the groove are hydrophobic. The groove is too narrow to accommodate duplex DNA without invoking a conformational change. However, the groove would be ideally suited to binding the phosphodiester backbone of ssDNA with the bases pointing away from the surface of the protein. In this way, the protein would present the DNA to allow homologous pairing with a complementary strand, thus promoting strand annealing. Hydroxyl-radical cleavage of ssDNA bound to both full-length RAD52 and $RAD52_{1–209}$ reveals an interesting pattern with a four-base periodicity (Fig. 2). An extension of 5–6 Å for each base separation, typical for the extended form of ssDNA, would allow DNA to follow the groove, giving a binding site of four bases per subunit, which would be consistent with the four-base repeat observed in the hydroxyl-radical footprinting. It has been proposed that residues 39–80 contribute to the DNA-binding region in RAD52 (18, 29). This region (highlighted in Fig. 4*B*) forms an extended hairpin that forms one side of the proposed DNA-binding groove.

A Mechanism for ssDNA-Strand Annealing. The mode of binding of ssDNA that we suggest, with the bases displayed outward, suggests a mechanism for annealing complementary strands (Fig. 5). One possibility is that strand annealing *in vivo* occurs by interaction of the RAD52–ssDNA complex directly with either an uncoated complementary ssDNA or one coated with RPA. It is known, however, that binding of ssDNA induces aggregation of RAD52 that can be observed directly by electron microscopy (12). Therefore, an alternative possibility is that with the ssDNA bound with the bases presented outward, two (or more) RAD52–DNA complexes could associate to facilitate pairing of the bases. If the sequences are complementary, then the interaction between the complexes will be stabilized, but if not complementary, the complexes could dissociate and then reassociate with other protein complexes. The nucleation length for duplex renaturation is three or four bases, which is in good agreement with the hydroxyl-radical footprinting that suggests a single RAD52 subunit DNA-binding site covers four bases. Once strand annealing is initiated, the two complexes could roll around each other, driven by the energetically favorable formation of the DNA duplex until the DNA becomes base-paired. The duplex DNA then may be released from the RAD52 ring, or alternatively release may require other protein factors. Specificity is achieved therefore by the favorable energy change that would accompany only the annealing of complementary sequences. It is noteworthy that this mechanism for ssDNA binding and strand annealing could be applied to RAD52 oligomers of virtually any size, with the proposed interactions being between individual subunits, irrespective of the overall size of the rings.

The structure of $RAD52_{1–209}$ that we present here suggests how the protein interacts with ssDNA and how it might promote strand annealing. However, RAD52 also interacts with RAD51 and RPA via the missing C-terminal domain, and it is hoped that future structural studies will provide molecular details for these interactions.

We thank the members of the S.C.W. and D.B.W. laboratories for suggestions; Jean-Yves Masson and Michael McIlwraith for providing RAD52; S. Sandler for providing plasmid pSJS1240; and the European Synchrotron Radiation Facility for access to beamlines. This work was supported by Cancer Research U.K. (formerly the Imperial Cancer Research Fund). Y.L. is a recipient of an American Cancer Society postdoctoral fellowship.

1. Game, J. C. (1983) in *Yeast Genetics: Fundamental and Applied Aspects*, eds. Spencer, J. F. T., Spencer, D. H. & Smith, A. R. W. (Springer, New York), pp. 109–137.
2. Petes, T. D., Malone, R. E. & Symington, L. S. (1991) in *The Molecular and Cellular Biology of the Yeast Saccharomyces: Genome Dynamics, Protein Synthesis and Energetics* (Cold Spring Harbor Lab. Press, Plainview, NY), Vol. 1, pp. 407–521.
3. Mortensen, U. H., Bendixen, C., Sunjevaric, I. & Rothstein, R. (1996) *Proc. Natl. Acad. Sci. USA* **93,** 10729–10734.
4. Shinohara, A., Shinohara, M., Ohta, T., Matsuda, S. & Ogawa, T. (1998) *Genes Cells* **3,** 145–156.
5. Sugiyama, T., New, J. H. & Kowalczykowski, S. C. (1998) *Proc. Natl. Acad. Sci. USA* **95,** 6049–6054.
6. New, J. H., Sugiyama, T., Zaitseva, E. & Kowalczykowski, S. C. (1998) *Nature* **391,** 407–410.
7. Shinohara, A. & Ogawa, T. (1998) *Nature* **391,** 404–407.
8. Sung, P. (1997) *J. Biol. Chem.* **272,** 28194–28197.
9. Baumann, P. & West, S. C. (1999) *J. Mol. Biol.* **291,** 363–374.
10. Benson, F. E., Baumann, P. & West, S. C. (1998) *Nature* **391,** 401–404.
11. Van Dyck, E., Stasiak, A. Z., Stasiak, A. & West, S. C. (2001) *EMBO Rep.* **2,** 905–909.
12. Van Dyck, E., Hajibagheri, N. M. A., Stasiak, A. & West, S. C. (1998) *J. Mol. Biol.* **284,** 1027–1038.
13. Stasiak, A. Z., Larquet, E., Stasiak, A., Müller, S., Engel, A., Van Dyck, E., West, S. C. & Egelman, E. H. (2000) *Curr. Biol.* **10,** 337–340.
14. Parsons, C. A., Baumann, P., Van Dyck, E. & West, S. C. (2000) *EMBO J.* **19,** 4175–4181.
15. Boundy-Mills, K. L. & Livingston, D. M. (1993) *Genetics* **133,** 39–49.
16. Asleson, E. N., Okagaki, R. J. & Livingston, D. M. (1999) *Genetics* **153,** 681–692.
17. Kagawa, W., Kurumizaka, H., Ikawa, S., Yokoyama, S. & Shibata, T. (2001) *J. Biol. Chem.* **276,** 35201–35208.
18. Park, M. S., Ludwig, D. L., Stigger, E. & Lee, S. H. (1996) *J. Biol. Chem.* **271,** 18996–19000.
19. Davis, A. P. & Symington, L. S. (2001) *Genetics* **159,** 515–525.
20. Kiltie, A. E. & Ryan, A. J. (1997) *Nucleic Acids Res.* **25,** 2945–2946.
21. Del Tito, B. J., Jr., Ward, J. M., Hodgson, J., Gershater, C. J., Edwards, H., Wysocki, L. A., Watson, F. A., Sathe, G. & Kane, J. F. (1995) *J. Bacteriol.* **177,** 7086–7091.
22. Otwinowski, Z. & Minor, W. (1997) *Methods Enzymol.* **276,** 307–326.
23. Weeks, C. M. & Miller, R. (1999) *J. Appl. Crystallogr.* **32,** 120–124.
24. Collaborative Computing Project No. 4 (1994) *Acta Crystallogr. D* **50,** 760–763.
25. Roussel, A. & Cambillau, C. (1989) *Silicon Graphics Geometry Partner Directory*, ed. Silicon Graphics (Silicon Graphics, Mountain View, CA), pp. 77–78.
26. Brunger, A. T., Adams, P. D., Clore, G. M., DeLano, W. L., Gros, P., Grosse-Kunstleve, R. W., Jiang, J.-S., Kuszewski, J., Nilges, M., Pannu, N. S., *et al.* (1998) *Acta Crystallogr. D* **54,** 904–925.
27. Sigurdsson, S., Trujillo, K., Song, B. W., Stratton, S. & Sung, P. (2001) *J. Biol. Chem.* **276,** 8798–8806.
28. Singleton, M. R., Sawaya, M. R., Ellenberger, T. & Wigley, D. B. (2000) *Cell* **101,** 589–600.
29. Ranatunga, W., Jackson, D., Lloyd, J. A., Forget, A. L., Knight, K. L. & Borgstahl, G. E. O. (2001) *J. Biol. Chem.* **276,** 15876–15880.
30. Nicholls, A. & Honig, B. J. (1991) *J. Comput. Chem.* **12,** 435–445.